Nanoscale

Sensitive Field-effect Transistor Sensors with Atomically Thin Black Phosphorus Nanosheets

Journal:	*Nanoscale*
Manuscript ID	NR-ART-11-2019-009354
Article Type:	Paper
Date Submitted by the Author:	03-Nov-2019
Complete List of Authors:	Maity, Arnab; University of Wisconsin Milwaukee Sui, Xiaoyu; University of Wisconsin Milwaukee Pu, Haihui; University of Wisconsin Milwaukee Bottum, Kai; University of Wisconsin Milwaukee Jin, Bing; University of Wisconsin Milwaukee Chang, Jingbo; University of Wisconsin Milwaukee Zhou, Guihua; University of Wisconsin Milwaukee Lu, Ganhua; University of Wisconsin Milwaukee Chen, Junhong; University of Wisconsin Milwaukee

ARTICLE

Sensitive Field-effect Transistor Sensors with Atomically Thin Black Phosphorus Nanosheets

Received 00th January 20xx,
Accepted 00th January 20xx

DOI: 10.1039/x0xx00000x

Arnab Maity,[a] Xiaoyu Sui,[a] Haihui Pu,[a] Kai J. Bottum,[a] Bing Jin,[a] Jingbo Chang,[a] Guihua Zhou, [a] Ganhua Lu[a] and Junhong Chen[a,b,c,]*

Atomically thin black phsphoorus (BP) field-effect transistors have excellent potential for sensing applications. However, commercial scaling of PFET sensors is still in early stage due to various technical challenges, such as tedious fabrication, low response% caused by rapid oxidation, non-ideal response output (spike/bidirectional), and large device variation due to poor control over layer thickness among devices. Attempts have been made to address these issues. First, a theoretical model for response% dependence upon number of layers is developed to show the role of atomically thin BP for better responses. A position-tracked, selected-area-exfoliation method has been developed to rapidly produce thin BP layers with a narrow distribution (~1–7 layers), which can harness the excellent gate control over PFET channel. The typical current on/off ratio is in the range of ~300–500. The cysteine-modified Al_2O_3-gated PFET sensors show high responses (~ 30–900%) toward a wide detection range (~1–400 ppb) of lead ions in water with typical response time of ~10–30 s. A strategy to minimize device variation is proposed by correlating PFETs' on/off ratio with sensitivity parameters. Thickness variation of gate oxide is investigated to explain non-ideal and ideal response transient kinetics.

1. Introduction

Since its discovery as a high-performance, two-dimensional (2D) layered material, black phosphorus (BP) has drawn considerable attention for application in sensors and digital electronics. [1-5] When exfoliated into mono- or few-layer sheets, BP can have a high current on/off ratio (~10^4) and a thickness-dependent energy band gap at room temperature. [6, 7] Thin BP has not only remarkable sensing properties due to its high surface-to-volume ratio, but also better field-effect transistor (FET) properties compared with graphene-based materials, which have also been extensively studied for the detection of heavy metals, bio-molecules, and gases.[8-11, 34]

Semiconducting nanomaterials with an atomically thin 2D structure are promising for FET sensors. [12,48] For a bulk crystal, the dangling bonds create unwanted phonon coupling and increase the number of interfacial states between the gate dielectric and the semiconducting channel, which thus creates poor gate electrostatics and degrades FET properties due to poor control over the entire bulk of the crystal. For atomically thin channels, however, charge carriers are confined in the very restricted region and thus can be controlled uniformly by gate voltage electrostatics, resulting in a better FET property. [12,48] Uniform control over the channel is crucial because the top-gate stimulus potential, which is generated by the interaction between the probe and target species, is usually very small and short ranged. An atomically thin 2D structure could provide enough signal-to-noise ratio, even for this very small potential caused by interactions between probes and trace amount of target analytes. Phosphorene (a single layer of BP) is a 2D semiconducting material with outstanding structural and electronic properties and could be a good choice for developing high-performance FET sensors. However, most studies have focused on its basic electronic characterization or sensing properties,[35-40] and are far from implementing a reliable and scalable technology (e.g., at the wafer level) to fabricate phosphorene FETs (PFETs), such as silicon-chip-level engineering. [13]

One challenge is to develop faster and reliable strategies for producing high-quality BP for scalable implementation in sensors and electronics. Various exfoliation methods for obtaining few-layer BP, including mechanical, chemical, ultrasonic, plasma-assisted, and laser-based exfoliation, [3, 14-17] have been reported with different advantages and disadvantages. Mechanical exfoliation could be ideal for rapidly producing high-quality sheets compared with other methods, but it lacks control over the thickness distribution, and identifying thinner flakes and then fabricating electrodes over flakes is time-consuming. Atomic force microscopy (AFM) can reveal the thickness distribution, but additional time is

[a] Department of Mechanical Engineering, University of Wisconsin-Milwaukee, Milwaukee, WI 53211, USA. E-mail: jhchen@uwm.edu
[b] Current address: Pritzker School of Molecular Engineering, University of Chicago, Chicago, IL 60637, USA. E-mail: junhongchen@uchicago.edu
[c] Current address: Argonne National Laboratory, Argonne, IL 60439, USA. E-mail: junhongchen@anl.gov

Electronic Supplementary Information (ESI) available: details of any supplementary information available should be included here. See DOI: 10.1039/x0xx00000x

needed for every device and BP quality may degrade during AFM characterization, thereby adversely affecting the FET properties and the subsequent sensing performance. The degradation of BP quality could be one of the reasons for the low response% observed in various PFET sensors previously reported. [4, 13] Therefore, it is desirable to develop a faster mechanical exfoliation strategy that can produce BP sheets with a narrow thickness distribution. In addition, the successful real-time implementation of PFET sensors also demands effective strategies to minimize device-to-device variation, avoid the degradation of BP from air/water exposure, and maintain a higher response and stable exponential response transient while eliminating non-ideal response transients, such as bidirectional or spike-like responses, which is often reported in the literature. [4, 18-20] This is unfavorable for real-time response computation and requires further investigation on the underlying mechanisms.

This article reports our attempts to address the technical challenges for PFET lead-ion sensors. We implemented a position-traced mechanical exfoliation strategy to accelerate the production of high-quality thin BP flakes with a narrow thickness distribution (1-7 L). Immediately after the selected-area exfoliation, BP flakes were transferred onto a silicon wafer with pre-fabricated gold electrodes (i.e., source and drain) to act as the FET channel, which significantly shortened the device fabrication time and helped to preserve BP quality. Note that fabricating the electrodes before the BP flake transfer reduced exposure of BP to air (avoid oxidation) and the chemicals used in microfabrication (e.g., photoresist, developer, etchant), thereby keeping the surface integrity and avoiding the additional electrode fabrication time needed for photoresist-based lithography, in which the flakes first need to be identified with a microscope.

The PFET sensors resulting from selected-area exfoliation exhibited a much higher current on/off ratio and excellent lead ion response compared with sensors resulting from thicker random-area-based BP flakes (> 10 L). PFET sensors from selected-area exfoliation may have current on-off ratios in the range of ~300–500 and high sensitivities (~30–900 %) in a wide concentration range of lead ions (~1–400 ppb). The limit of detection (LOD) is as low as 1 ppb with 30-70% response. A theoretical model was developed using the metal–oxide–semiconductor field-effect transistor (MOSFET) structure for the layer-dependent band gap combined with a band-bending model near the channel-oxide interface to explain the better response for the atomically thin FET channel. The band diagram of the channel-gate interface shows that the surface charge on the channel from the top-gate-induced positive field is proportional to the band-bending, and holes are depleted from the channel to create an electron-rich region. When the thickness of BP becomes comparable to the depletion width of the channel, a high response is expected due to excellent gate control by harvesting the minority charge carriers.

The relation among response%, concentration, and fitting constants correlates with current on/off ratios of various PFETs. It could be correlated with a broad-range device through a unique calibration equation, and this can be an indirect way to address the device variation issues. PFETs need an insulating top gate layer to ensure a stable on/off ratio and stable device performance in open ambient. [21] Here, we studied the influence of the gate oxide thickness on the response transients: non-ideal (e.g., bidirectional or spike-like due to multiple mechanisms) and ideal (unidirectional due to a single mechanism). Using the Langmuir adsorption mechanism, we propose a model to explain the influence of gate oxide thickness (0–5 nm) on the response pattern for lead ion sensing with the superposition of effects, including electrostatic gating, charge transfer (leakage), and lead ion diffusion time in water.

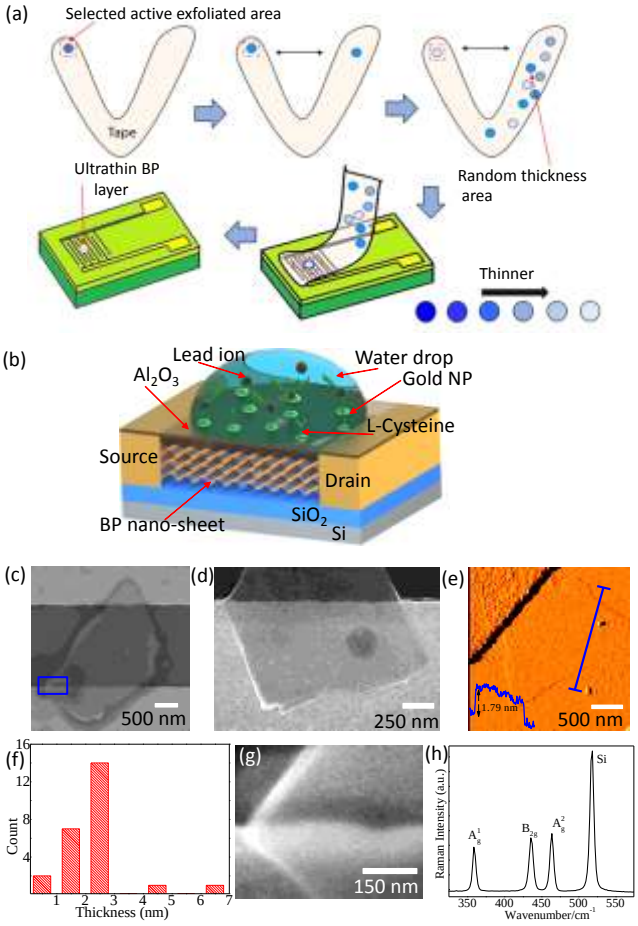

Fig. 1. (a) Schematic of the selected-area exfoliation of BP flakes into ultrathin BP nanosheets. (b) Model of the fabricated PFET sensor. (c) Low- and (d) higher-magnification FESEM images of a BP nanosheet from a selected-area exfoliated sample. (e) AFM image of a BP nanosheet (inset: thickness profile). (f) Thickness distribution of BP nanosheets from a typical device, shown in Supporting Information Figure S1a. (g) High-magnification FESEM image of BP/ALD/Au to visualize the Au nanoparticles on the surface. (h) Raman spectrum of typical BP nanoflakes.

2. Results and discussion

2.1 Selected-area Exfoliation of BP and the Fabrication of ALD-Gated PFET Sensors

We developed a significantly improved mechanical exfoliation method, namely selected-area exfoliation, to consistently obtain very thin layer BP sheets (1–7 layers). The exfoliation process is shown in Figure 1a and Supporting Information Video 1. First, a larger BP flake is attached to the adhesive side of transparent scotch tape, and the location of the flake is marked (i.e., selected area) with a red marker on the non-adhesive side of the tape (i.e., the back side of the tape). The exfoliation is then carried out repeatedly with other adhesive parts on the tape. For each exfoliation, the selected marked area is brought in contact with a completely fresh site on the adhesive tape and then gently separated; in this way, the BP flakes on the selected area become systematically thinner and the color of the BP on the selected area becomes lighter with more exfoliation cycles. After 20-25 cycles, only thin BP sheets remain in the selected area and are ready to be transferred onto interdigitated Au electrodes prefabricated on an Si wafer using the standard lithography process that we have reported previously. [22] It should be noted that the other parts on the tape used for exfoliation have various thickness distributions (as can be seen from the distribution of brighter and lighter patches) which are unsuitable for making high-performance FETs.

The Si wafer surface is cleaned by oxygen plasma followed by heat treatment. Once the selected-area exfoliation is finished, the selected area on the tape is pressed against the sensor's finger electrode surface for some time, as shown in Figure 1a, and then the tape is gently removed from the wafer surface. The mark on the back of the tape guides the proper transfer and ensures the transfer of thin BP nanosheets onto the wafer to bridge the interdigitated Au electrodes for constructing the FET channel. Immediately after transfer, the sensor is annealed in an Ar environment at 200 ºC for 1 hr to lower the contact resistance. After that, the sensor is quickly placed into an atomic layer deposition (ALD) chamber to deposit a thin layer of Al_2O_3 as the top gate of the PFET. The top gate passivation is used to protect BP from oxygenated species and maintain its electronic properties. The Al_2O_3-coated FETs are sputter-coated with Au nanoparticles to provide surface active sites for chemical probes. The whole device configuration is shown in Figure 1b.

We used L-cysteine as the probe molecule attached to the Au nanoparticles through the -SH group. It is reported that the -COOH group from cysteine can bind with lead ions in the solution, and cysteine was previously used for lead ion removal/sensing.[23] With this FET structure, a wide range of lead ion testing has been carried out for both ultrapure water and tap water as background.

2.2. Morphological, Surface, and Spectroscopic Characterization of 2D BP Crystal

Figure 1c and d show the field-emission scanning electron microscopy (FESEM) images of a typical BP nanosheet from the selected-area exfoliation that connects the electrodes. It is apparent that the surface of the BP nanosheet is devoid of any visible protuberance, suggesting the surface ALD layer successfully prevented further oxidation of the nanosheet, which is consistent with the literature. [21] It should be noted that most flakes in the sensing area showed uniform surface morphology.

Atomic force microscopy (AFM) was used to further verify the surface morphology, uniformity, and thickness distribution of the BP flakes. Figure 1e shows an AFM image of the ultrathin BP nanosheet with its thickness profile. The typical thickness distribution across the device was found as ~ 0.8–6.23 nm (additional AFM images and thickness profiles can be found in Supporting Information Figure S1a). A very narrow thickness distribution (1–7 layers) of the BP sheets could be realized using the selected-area exfoliation process (Figure 1f). In contrast, BP flakes from the unselected sites on the tape were generally much thicker and had a very non-uniform thickness distribution (see Figure S2a-b in Supporting Information). Figure 1g shows the FESEM image of Au nanoparticles uniformly distributed on the ALD-coated PFET, which are used to link the chemical probes. Figure 1h shows the typical Raman spectra of the samples from selected-area exfoliation. The peaks around 359 cm^{-1}, 436 cm^{-1}, and 464 cm^{-1} can be assigned to one out-of-plane mode (A^1_g) and two in-plane (B_{2g} and A^2_g) Raman modes for BP, respectively. These peaks signify the excellent crystallinity of the BP flakes and match well with the results in the literature. [16] A first-order Si peak at ~520 cm^{-1} is also observed from the background Si substrate.

2.3. Theoretical Modelling of the Thickness-Dependent Response Pattern for BP FET Sensors

BP is a semiconductor with a layer-dependent direct band gap which creates variability in the current on/off ratio. The higher current on/off ratio is promising for FET sensors, since their sensing properties are controlled by potential (or charge (ΔQ)) induced by an electrostatic, receptor-ligand interaction, or antigen-antibody interaction. Monolayer phosphorene has the largest transport band gap (E_g) (~2.0 eV) and the highest current on/off ratio, and the increase in layer numbers decreases the band gap as well as the on/off ratio. [7, 24, 32] A proportional relationship between the band gap (or layer number) and the measured current on/off ratio for BP can be found elsewhere. [32] Therefore, the minimum layer number is desired to reach a higher on/off ratio, which could help to achieve higher response% for dielectric-gated PFET sensors, but carrier mobility could degrade for very thin BP due to scattering from defect sites at the interface between the substrate gate oxide and the BP channel. [6] For extremely low thickness (one or two layers), since the band gap is larger, greater noise is also present for channel material or larger voltage is required to drive the current. Therefore, the optimum thickness range for BP could exist for the desired on/off ratio and mobility and thus results in a maximum response. For instance, we previously demonstrated a volcano-shaped profile for the response of BP FET gas sensors versus BP thicknesses, with response maxima near 6 layer; i.e., the response of the BP gas sensors is significantly higher for 4- to 7-layer BP and decreases for either smaller (1-4 layers, due to degraded mobility) or larger thicknesses (> 7 layers, due to a smaller band gap). [3] For a BP gas sensor or a bare FET sensor, the channel material is directly exposed to gases or analytes. The situation is different for the dielectric-gated PFET heavy-metal sensor, which, presumably, is controlled entirely by gate-induced charge during sensing and has no leakage current through the gate oxide. concentration on the

surface is dominated by electrons whereas carrier concentration of the bulk BP crystal is still hole. Due to band-bending near the surface of the

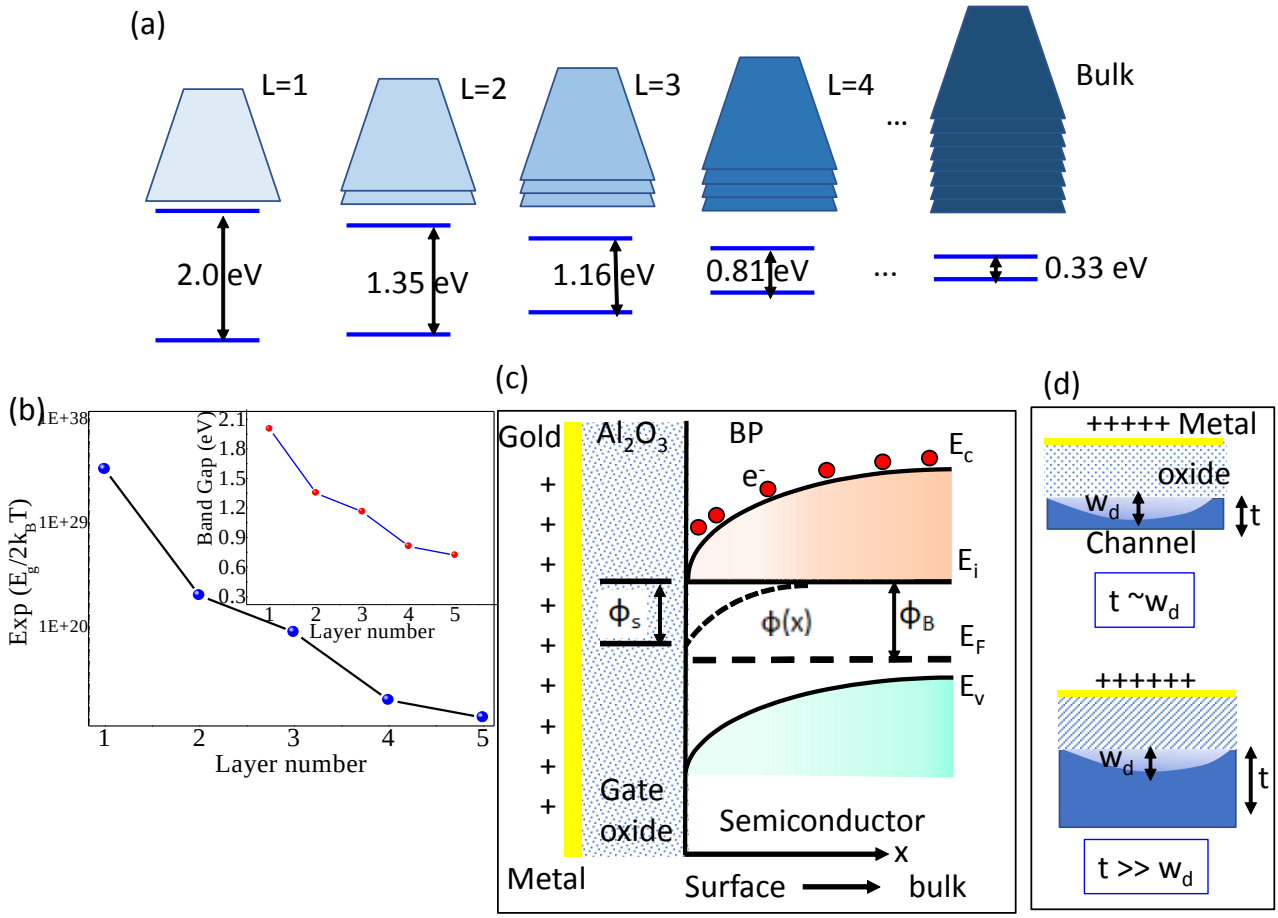

Fig. 2. (a) Model of the layered structure of BP and its layer-dependent band gap. (b) Plot of layer-dependent band gap vs. thickness from references [6, 24] (shown in inset) to calculate $R \sim exp\ (E_g/K_BT)$. (c) The metal oxide-semiconductor band diagram for BP/Al_2O_3/Au system under positive voltage bias. (d) Schematic of the comparison of two cases for t ~ w_d and t >> w_d.

oxide-BP interface, the bulk potential (Φ_B, due to the acceptor concentration from intrinsic p-type semiconductor) and surface potential (Φ_S, due to the electron from positive top-gate-induced band-bending) should be different. Therefore, E_i and E_F in Eq. 1 can be expressed as, [25]

$$\boldsymbol{\Phi_B = E_{i\_bulk} - E_{Fp\_bulk}} \quad (2)$$

$$\boldsymbol{\Phi_S = E_{i\_surface} - E_{i\_bulk}} \quad (3)$$

Thus, for the BP gas sensor or bare FET sensor, carrier mobility should be directly influenced during sensing due to the charge transfer as a result of the direct contact with the analytes (gas/solution), whereas carrier mobility for the dielectric-gated PFET heavy-metal sensor should be invariant during sensing due to the presence of the top gate oxide. The response% (R) of an FET sensor can be approximated as,

$$\boldsymbol{R = \frac{I_{ds} - I'_{ds}}{I_{ds}} \sim \exp(E_g\ /2k_BT) \cdot \exp(|E_i - E_F|/k_BT\ )} \quad (1)$$

where I_{ds} and I_{ds}' are current values in background DI water and lead ion solution, respectively, and E_g, k_B, T, E_i, and E_F are the band gap, Boltzmann constant, temperature, intrinsic energy, and Fermi energy, respectively. The detailed derivation of the equation can be found in Supporting Information 4. Eq. 1 clearly shows that response (R) increases for thinner BP with a larger band gap (E_g). The term $exp\ (E_g/2k_BT)$ is extremely sensitive to BP thickness, even for single-layer variations.

Using the literature results,[24] a schematic model for BP layer-dependent variation of band gap and a semi-quantitative plot for response% versus thickness are shown in Figure 2a and b, respectively. The model indicates that a small change in band gap caused by layer variation can affect the response, particularly in the atomically thin region. To illustrate the effect of the term $\boldsymbol{\exp(|E_i - E_F|/k_BT\ )}$ in Eq. 1, the gate oxide (Al_2O_3) - semiconductor (BP) band alignment under positive gate bias is shown in Figure 2c.

When the top gate becomes positive due to the adsorption of lead ions, negative charges (electrons) are introduced on the surface of the channel, which transitions from depletion to inversion upon further increase of the top gate positive electrostatic field. Due to the top gate positive field, the carrier. The electron concentration

can be written as $n = n_i \exp(E_F - E_i)/k_BT$. For the p-type surface semiconductor, p >> n and the electron concentration at the

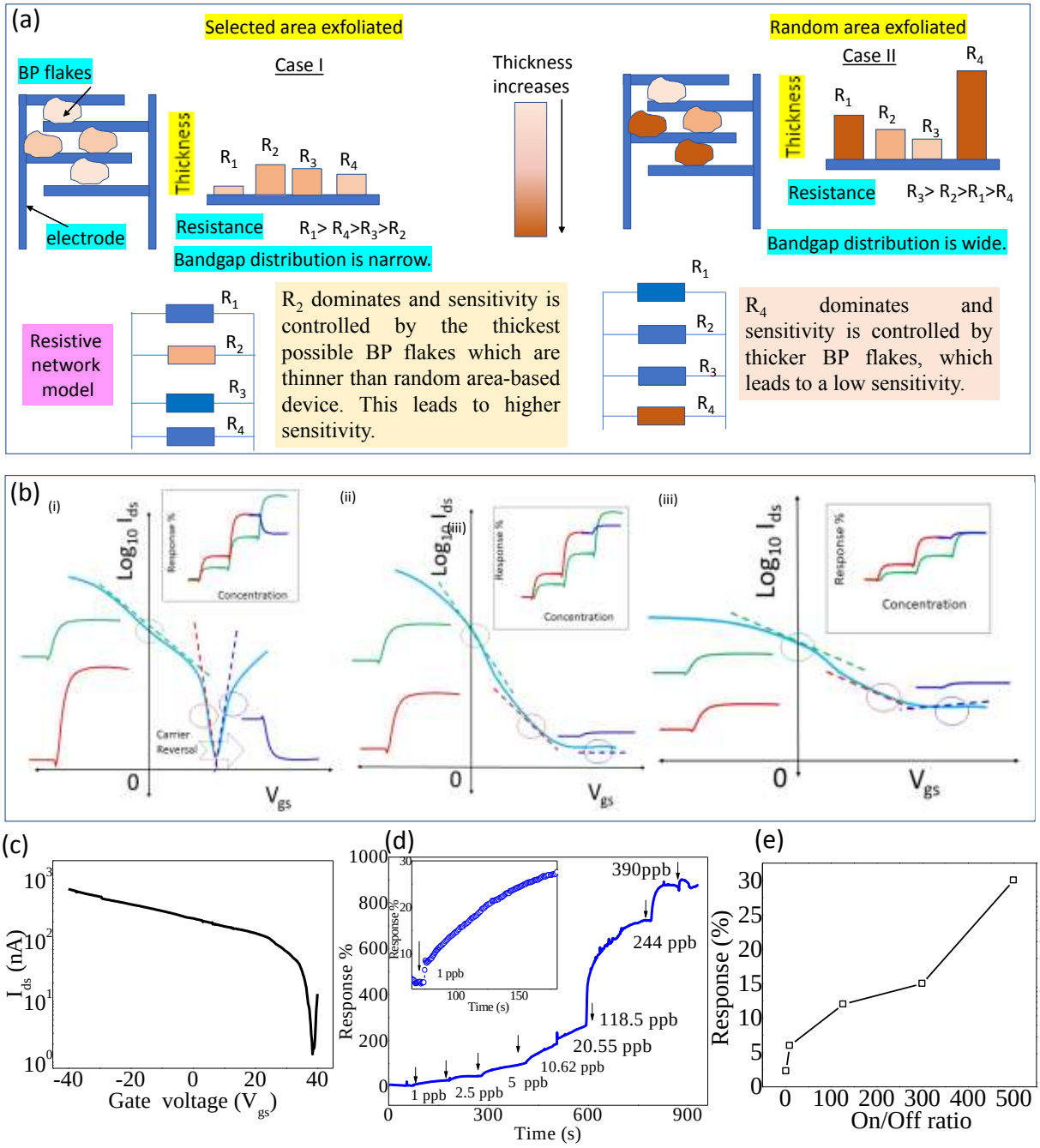

Fig. 3. (a) The models of BP flake distribution; Case I: selected-area-based device, and Case II: random-area-based device. (b) The model schematic and expected response transient direction (inset) of the V_{gs}-I_{ds} curve for (i) high, (ii) medium, and (iii) low on/off ratio. (c) Plot of V_{gs}-I_{ds} characteristics curve for V_{ds} ~ -0.01 V and V_{gs} ~-40 V to 40 V. (d) Typical responses to lead ions for selected-area-based sensor with on/off ratio ~500; the response transient for 1 ppb lead ion is shown in the inset. (e) Plot of typical on/off ratio vs. response% for various devices for 1 ppb lead ion concentration.

(n_s), due to gate-induced band-bending, can be written using Eq. 2 and 3.

$$n_s = n_i \exp(\Phi_S - \Phi_B)/k_BT \quad (4)$$

Here, $\Phi_S - \Phi_B$ represents the amount of band-bending near the surface. Eq. 4 indicates that an increase in the induced surface electronic charge (n_s) causes a higher relative current change by enhancing the response. When the transistor is operated in the

depletion region (for the small positive gate), the number of holes (p) becomes smaller than the actual bulk acceptor concentration (N_A) due to the induced surface electronic charge by depleting holes from the surface ($n_s < N_A$). The depletion width (w_d) of the channel from the oxide-BP interface extends to the bulk BP. The surface potential distribution ($\boldsymbol{\Phi}(\boldsymbol{x})$) can be expressed as, [25, 26]

$$\boldsymbol{\Phi}(\boldsymbol{x}) = \boldsymbol{\Phi_S}(\mathbf{1} - \frac{x}{w_d})^2 \quad (5)$$

where $\boldsymbol{\Phi_S} = \frac{e^2 N_A w_d^2}{2\varepsilon_0 \varepsilon_r}$. From these relations, $\Phi(x)$ reaches the maximum ($\sim\boldsymbol{\Phi_S}$) when x = 0 (i.e., just at the surface) and systematically decreases when x increases. Here, x can be considered the channel thickness (t) (see Figure 2c). In other words, when the BP channel becomes atomically thin, the depletion effect will be better, resulting in excellent gate control and a higher relative current change (higher response). For the bulk BP sheet (the thickness of sheet (t) is much higher than w_d), the extent of depletion is limited only to the surface and thus poor gate control over the entire crystal, which then exhibits a lower relative current change (lower response). Figure 2d shows the schematic representation of these two cases ($t \sim w_d$ and $t >> w_d$).

2.4. Electrical Characteristics and Lead Ion Sensing Measurements of PFETs with BP from Selected-Area Exfoliation

Using the exfoliation strategy currently available in literature, it is still not possible to precisely control the specific thickness of a BP nanosheet for each FET device. It is also unreasonable and very time-consuming to find the specific exfoliated flakes microscopically and then fabricate the electrodes for every device. Therefore, it would be desirable if we can work with a narrow distribution of thicknesses as optimum as possible. As per the quantum size effect, the thinnest distribution of BP flakes could exhibit a tunable band gap as well as current on/off ratio. Also, the effective number of layers could be roughly estimated from the measured on/off ratio, which could be calibrated with the measured response% of the sensor. In our FET sensors, instead of a single sheet we used a network of thin BP sheets with a narrow thickness distribution. The sheet thickness distribution was found to be 0.8–6.23 (1–7 layers) (Figure 1f), which is very close to the specified region optimum for obtaining low noise and the optimum on/off ratio. This is because the conduction path or the response% contribution is dominated by the thicker flakes (6–7 layers, with lower resistivity), as they form the least-resistive paths compared with the thinner flakes (1–3 layers, with higher resistivity). The fabricated device should be selected based on the higher on/off ratio that could be achieved with the selected-area exfoliation strategy.

Figure 3a shows two models for thickness distribution across the interdigitated electrodes: Case I: devices from selected-area exfoliation; Case II: devices from random-area exfoliation. The response was found to be maximum for Case I, where top-gate-induced potential could have excellent control over the gate electrostatics due to the narrow thickness distribution of the thin BP flakes. The short-range stimulus on the top gate from the probe species would have a maximum effect (current change in channel) when the channel is atomically thin. For Case II (random area), since the thickness distribution is much wider and thicker flakes are dominant, band-gap tuning is unlikely due to the bulk nature (lowest band gap). Therefore, current will be bypassed (i.e., the short-circuit effect) through relatively thicker BP flakes, resulting in a lower on/off ratio and minor response due to poor gate electrostatic control over the bulk of the crystal. Eventually, any sensing effect from the thinner flakes cannot be captured, as they are circumvented because of the higher resistance even though they are present in the active area.

It also should be noted that subthreshold swing (SS) is another important factor for controlling the response of the FET sensor. Here, SS is defined as the inverse slope of the I_{ds}-V_{gs} curve in the subthreshold region and signifies the required gate voltage for change in current by one order of magnitude or a decade (SS ~ $dV_{gs}/d\,(log_{10}\, I_{ds})$). SS can be expressed as,

$$SS = dV_{gs}/d\,(log_{10}\, I_{ds}) \quad (6)$$

It is obvious that by lowering SS, more effective change of the current or response% could be achieved. It was reported that a higher response could be reached when a transistor is operated in the threshold region where I_{ds} changes exponentially with V_{gs}.[27] However, this is only valid when the channel maintains a unipolar conduction pathway (either n- or p-type, but not both) within the gate voltage range. If ambipolarity is found during the transistor operation, the channel could be switched from p-type to n-type by crossing the charge neutrality point (see the cartoon in Figure 3b (i)), which leads to a complete ambiguous current signal change in the direction opposite of the expected response change as the majority charge carrier is altered (see the response direction (red and blue curves) in the inset of Figure 3b (i)). Specifically, most layered materials, such as BP and MoS_2, show ambipolarity behavior during gate voltage sweeping; therefore, although the SS region is promising for a better response%, it may not be reliable for stable sensor operations. In addition, due to sensing signal drifting, the sensor can eventually cross the SS region and the sensing signal can behave completely opposite to the desired direction, leading to confusing feedback for analyzing the controller circuit and algorithm responsible for quantifying various species. For the second case (Figure 3b (ii)), the current saturates after threshold voltage and the sensing signal saturates for high-concentration analytes, leading to a limited detection range. The suppressed response behavior (blue line) can be observed when it crosses the threshold voltage limit.

For the third case (Figure 3b (iii)), the sensing performance could be suppressed if the current on/off ratio is smaller than that in previous two cases. If the inverse slope of $log_{10}I_{ds}$-V_{gs} is very small, then a higher gate voltage is needed to obtain an appreciable change in drain current. The top gate voltage generated by analytes is insufficient for moving the current to a greater extent, leading to a very small response. Specifically, this situation occurs when the off current value could not be lowered or completely off due to a variety of reasons, such as higher flake thickness, small band gap, and thermal limit. We will explain this point later in this article when the sensing performance of selected-area BP sensors is compared with random BP devices and another p-type 2D material, i.e., reduced graphene oxide (rGO). Although most reports showed a higher response in the near SS region for a single concentration, there is limited information about the wide-range concentrations that are the electronic equivalent to a wide range of top gate

voltage. Therefore, it is apparently safe to operate FET sensors in the linear region where the unipolar conductivity behavior is relatively well maintained for a wide voltage range operation (wide-range sensing capability, unidirectional response transients).

Figure 3c shows the measured drain current (I_{ds}) for a wide range of back-gate voltage (V_{gs} -40 V to 40 V). The typical current on/off ratio for this device (with ~300 nm-thick back-gate SiO_2) was ~500 for hole conduction. Due to this very high oxide thickness, large-gate voltage is needed to turn the FETs on or off. However, as the sensing event occurs through top gate (3–5 nm-thin Al_2O_3 dielectric layer, dielectric constant ~ 9.5), very small voltage from the top-gate stimulus response would be enough to change the current in the ultrathin BP channel. In addition, top-dielectric materials can segregate the measurement electrode from liquid analytes. We will discuss later the effect of the top-gate layer on sensing performance using kinetic analyses.

The plot of $\log_{10} I_{ds}$ versus V_{gs} shows clearly different operation regions according to the slope and direction of I_{ds}-V_{gs}. When V_{gs} is largely negative (near -40 V) the BP channel is electrostatically doped by hole, which is injected by the source electrode. This current has two components: thermionic emission current over the top of the Schottky barrier, and the tunneling current through the Schottky junction barrier potential. When the back gate is swept towards a less negative value, the second component (tunneling) starts to decrease while only the thermionic emission current prevails. This leads to a systematic decrease in current until it reaches the flat-band condition (where $d(\log_{10} I_{ds})/ dV_{gs}$ changes with different slopes). In this situation, the current becomes thermionically controlled until it reaches the charge neutrality point and decreases sharply with the slope nearly unchanged. This in turn gives a small SS value (~1.6 V/dec) near the subthreshold region compared with the linear region (~50 V/dec). It should be noted that the SS value in the linear region is not a real threshold swing but a simple calculated inverse slope of $d(\log_{10} I_{ds})/ dV_{gs}$ to compare the situation for both cases. A further increase in gate voltage leads to the lowest off-state current (charge neutrality point (CNP)) and then the device is switched to the electron-doped state. The CNP state is the result of both the hole and the electron current. The calculated current on/off ratio for the selected-area exfoliation method varied from 300–500 and the value decreased to < ~20 for the transferred random-thickness-area-based sample. The typical V_{gs}-I_{ds} curve for random-area samples is provided in Supporting Information Figure S3.

Figure 3d shows the real-time dynamic testing plot of a sensor (with BP from selected-area exfoliation and with a current on/off ratio ~501) for lead ions with various concentrations. The sensor had an LOD down to 1 ppb with ~30% response and responded to concentrations up to 390 ppb (with ~900% response). This sensing performance is effective for detecting the danger limit for lead ions (~15 ppb per EPA) in drinking water quickly and easily. Figure 3e shows the response dependence on the current on/off ratio in the linear region. As expected, a higher response could be achieved with a higher on/off ratio. A comparison of performance with various BP FET sensors in the literature is summarized in Table S1 of Supporting Information, which shows that the sensor in the present study features a better on/off ratio and a higher response than those reported in the literature. To verify their selectivity, the PFET sensors were exposed to various heavy-metal ions and other common metal ions both individually and mixed in solutions. Figure 4a and b show the dynamic responses of the PFET sensors for ~20 ppb mixed ions and ~100 ppb of various heavy-metal ions (Cd, Hg, As) with other common metal ions (Mg, Na, Fe, Ag). The PFET sensors showed minimal responses toward these ions except for lead ions, which suggests their excellent selectivity. Figure 4c shows the comparative response% plot for lead (15 ppb) with mixed ions (20 ppb) and individual (20 ppb) solutions of other metal ions. This potentially shows the present system can be applicable for both higher response and better selective lead ion detection in drinking water. As the isoelectric point of cysteine is ~5.02, the overall charge distribution remains negative when it is exposed to ultrapure water (pH~ 6-7). When the Pb^{2+} ions are attached to the cysteine probes through -COOH groups, the net positive charge creates an electrostatic gating at the top gate and modifies the current in the channel. The cysteine-based proteins/peptides, e.g., metallothioneins and phytochelatins, have been reported for toxic heavy metal removal from the cells and tissues.[41] Thus, cysteine and glutathione (GSH), have sepcial affinity with lead and other heavy metals through chelating reactions.[42-44] Particularly for L-cysteine, it is reported that lead can bind to various highly stable chelating complexes under varying pH conditions.[45] These include tridentate ligands, binding through the thiolate (−S−), carboxylate (−COO−), and amine (−NH_2) groups. These stable complexes could be: $PbH(Cys)^+$, $Pb(Cys)$, $PbH(Cys)^{2-}$, $PbH(Cys)^{--}$. It is generally found that most negative complex formation is highly favorable in higher pH (i.e., in alkaline media). Upon the decreasing pH, these become neutral complexes and positive complexes (at neutral and lower pH (i.e., near acidic). In our experiments, we have used DI water as the solution media for FET sensing tests. Due to absorption of environmental CO_2 gas, the DI water becomes mildly acidic in nature 5.5-6 and this is a favorable condition for formation of positive complexes at the sensor surface by creating a +Ve gating effect.

The selectivity of -COOH in cysteine for lead ions is mostly due to the different electronegativity/affinity of metal ions, of which heavy metal ions usually have larger values. In this reference,[46] experimental characterization has been carried out using NMR technique to study the chemical shift changes of C13 atom in GSH towards different metal ions. In this work, it was found that order of affinity at various binding sites is: $Pb^{2+} > Cd^{2+} > Zn^{2+}$, which is just in agreement with their order of electronegativity. The electronegativity of lead (2.33) is much higher than other metal ions such as Mg (1.31), Zn (1.65), Na (0.93), and Cd (1.69). The structure of the cysteine is just similar with GSH that includes, -SH, -COOH, -NH2 groups. Therefore, cysteine-Pb interaction could create much stronger positive field than the cysteine-other_metal_ions. Some other report could be found for selective lead ion detection using cysteine probes.[23]

For Hg^{2+}, it is a bit tricky here since the electronegativity of Hg is larger than Pb, and thus -COOH-Hg has stronger interaction than -COOH-Pb. However, in either cysteine or GSH, -COOH is accompanied closely by NH_2, which is positively charged into NH_3^+ in ultrapure water (pKa >9) which is mild acidic due to

environmental adsorption of CO_2. While Pb only binds with -COOH into -COO-Pb with 2 positive charges introduced by Pb, Hg binds with -COOH and $-NH_3^+$ complex and $-NH_3^+$ is deprotonated into NH_2 forming $-COO-NH_2$-Hg with reduced positive charges introduced by Hg. Therefore, the surface voltage change from Pb adsorption should be larger than Hg. This might explain why TGA probe (HS-CH_2-COOH, with only -COOH) is better for Hg detection than Pb, while other amino- ($-CH_2-NH_2$-COOH) containing probes (either GSH or cysteine) are better for Pb rather than Hg.[47] A schematic model is shown in supporting information 10 (Fig. S8).

We also used Milwaukee tap water spiked with lead ions in various concentrations to demonstrate the concept for real-water analysis (see Supporting Information Figure S4). The real tap water testing shows that the sensors are not affected by other common metal ions, even though they can be present with higher concentrations (several ppm), and could be effective for lead ion testing in tap water. The response time was found to be a little longer than the lead-spiked ultrapure water response transients, possibly because the presence of high-molar common metal ions in lake water may slow lead ion diffusion to the surface of the sensor. In our future work, we will continue to improve this result. A separate study for sensing test without cysteine (BP/Al_2O_3/Au) is shown in supporting information 9 (Fig. S7). This shows that there is almost negligible response towards lead with this configuration, suggesting the role of cysteine for capturing lead selectively.

2.5. Comparison with Random-Area-Based PFET Device and rGO-Based Sensor

To verify the importance of a higher on/off ratio for achieving a greater response with the PFET sensors, control experiments have been carried out with random-area-based PFETs and rGO-based FETs. The details of the rGO deposition can be found in our earlier work [9] Figure 4d shows the dynamic response to lead ions from a typical random-area-based device. Figure 4e compares the response versus the lead concentration for FETs based on selected-area and random-area BP and rGO while keeping device configuration the same. The selected-area PFET sensor showed a much higher response than the random-area-based sensor and rGO device, which can be attributed to the much higher on/off ratio for selected-area PFETs (~300-500) than random-area PFET (5-10) and rGO FET (1.5-2) (see Supporting Information Figure S3 and S6). In addition, the SS values for both random-area PFETs and rGO FETs are even much higher than the selected-area PFETs in the linear region. The lower on/off ratio for rGO FETs could be related to the band gap variation. The oxygen content (C:O) plays an important role for tuning the band gap of rGO. It was reported that for a typical 5-10% oxygen content, the band gap of rGO can vary from ~0.2-0.3 eV, [28] whereas, the band gap for thin-layer BP could be ~ 0.3-2.0 eV. For a smaller band gap, the potential barrier between the source and the drain is lower and the low-energy charge carrier can tunnel from one end to the other. This causes off-state leakage current to uplift and the on/off ratio becomes smaller as the SS value increases. The sensors with selected-area exfoliated BP comprised of thin BP nanosheets with a narrow thickness distribution have a much higher on/off ratio than the random-area-based sensors. Thinner layers with more uniform thicknesses provide higher band-gap distributions, which signifies a lower off-state current by decreasing the drain source leakage current, resulting in a higher on/off ratio as well as smaller dV_{gs}/dI_{ds}; these factors lead to a very high response. For a random thickness sample, the average thickness is much higher, and the thickness distribution is wider, resulting in the addition of tunneling current due to lower band gap distribution. This increases the off-state current by degrading the on/off ratio and SS value required for sensing. For rGO, even though the thickness is single-layer and maintained very well (see Supporting Information Figure S5 a and b) without any layer flocculation due to our improved functionalization strategy, its band gap is smaller than BP, as previously described. This results in a higher off-state current. The typical V_{gs}-I_{ds} curve is shown in Supporting Information Figure S6. When comparing V_{gs}-I_{ds} curves for each case, both the SS value and the current on/off ratio of PFETs with selected-area BP are much better than the random-area-based BP devices and rGO-based devices for demonstrating a better sensing platform. It is also expected that an extremely high response% per unit change of concentration could minimize the device variation issues with less error for predicting unknown concentrations.

2.6 Device Variation Minimization and Sensor Calibration for Wide Range Devices

The PFET sensor with a very high response is promising for real-life applications; however, before its successful practical application, it is crucial to realize large-scale fabrication of PFETs with a minimum device-to-device variation. Until now, this level of scaling with BP devices is not achieved like present-day silicon technology, since a very uniform channel thickness is required for every FET on a large scale. Some strategies, such as coding, have been adopted for commercial glucose sensors to manage sensor variations [29, 30]. Coding is the process that “teaches” the glucose monitor to recognize a batch code encrypted in each test strip to ensure accurate results. Glucose sensor manufacturers make the

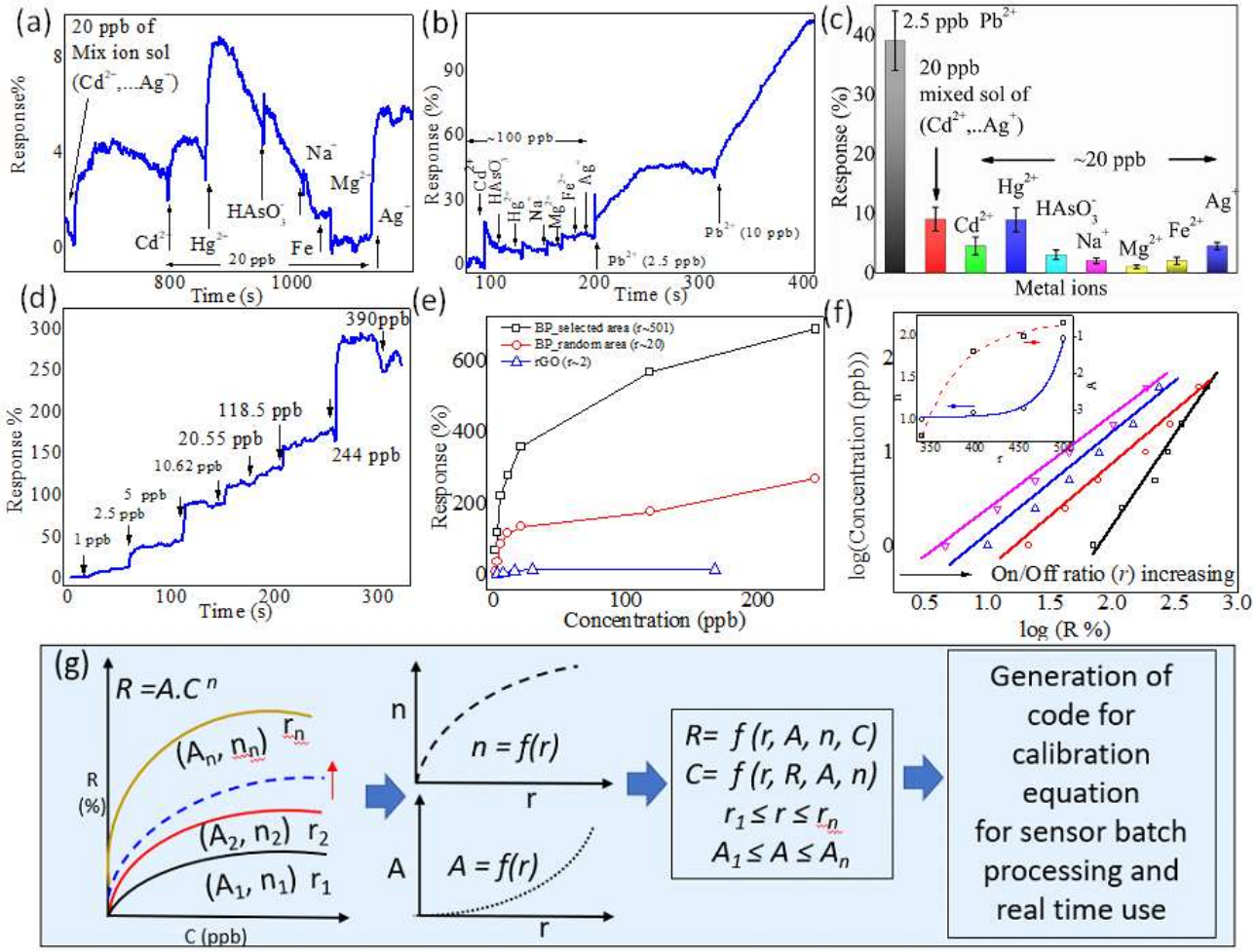

Fig. 4. The response transient for (a) various common metal ions and (b) lead ion in various mixed-ion backgrounds mimicking the real situation. (c) The calculated response% for various metal ions compared with lead to demonstrate the selectivity. (d) The lead ion response of random-area-based PFET when keeping other experimental parameters the same. (e) The comparison of lead ion responses between selected-area-based PFET, random-area-based PFET and rGO FET. (f) The experimental (dotted) and fitted (linear) data for log(response%) vs. log (concentration) for various current on/off ratios (r~300-500). The inset shows the calculated values of A and n fitted with r. (g) Schematic of the sensor calibration for a wide range of devices with the response R=f(r, A, n, C) for sensor batch processing.

unique calibration for each batch of sensors, and a specific code is generated and installed into the memory of the hand-held glucose meter. When a certain sensor is ready to test, users just need to provide a numeric code to the meter, and the meter will be informed automatically about the batch from which the sensor is taken. The controller in the meter will pick up the predefined calibration equation from its memory to predict glucose level in blood.

This coding approach could be useful for our PFETs devices. In our case, the measured current on/off ratios for various devices have been correlated with the sensing performance (calibration curve between concentration (C in ppb) and response (R%)) in the following relation:

$$\boldsymbol{R = AC^n} \quad (7)$$

where *A* is a constant and *n* is the sensitivity. Naturally, if *n* is higher, the response will also be higher. The relation can be simplified as $\boldsymbol{log\ (R) = log\ (A) + n\ log\ (C)}$ (8)

The relation could be fitted with different current on/off ratios (r) for various samples and calculated constants (*A* and *n*) have been correlated with *r*. Figure 4f shows the response versus concentration plot for different *r* values (values of n and A are plotted in the inset). With the increase of the on/off ratio, *n* and *A* also increase. This relation could be fitted with an exponential function, and the values of *n* and *A* could be estimated using this calibration for any arbitrary sample with a specified on/off ratio in a certain range of interest. Once this is achieved, the sensor's calibration for predicting unknown lead ion concentration could be used from calculated response% using the equation. Figure 4g shows the schematic of the proposed calibration strategy for PFET

sensors. Using selected area-based PFET sensors, the response% could be made higher by taking advantage of

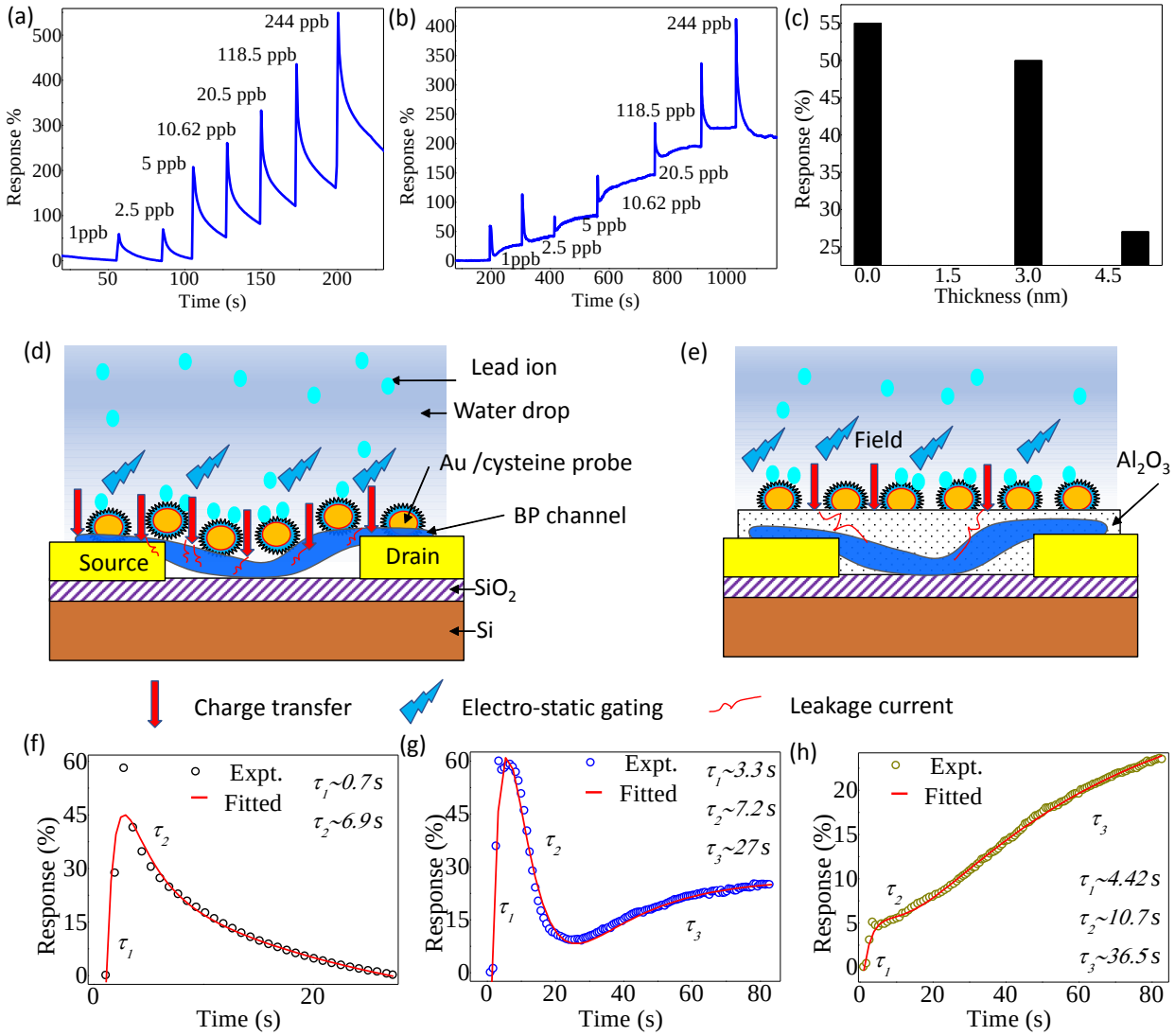

Fig. 5. Response transients of the BP FET sensors with (a) 0 nm and (b) 3 nm ALD layer thicknesses. (c) The thickness effect on response for 0-5 nm ALD samples to 1 ppb lead ion sample. Schematic model for the PFET sensing mechanism for (d) without and (e) with ALD. The experimental (dotted) and fitted (line) response transient for 1 ppb lead ion solution with (f) 0 nm, (g) 3 nm, and (h) 5 nm ALD thickness.

ultrathin nature of BP flakes. Subsequently, device variation minimization could be encountered with prior knowledge of *r, A, n, c,* where *R=f(r, A, n, c).* More accurate and generalized calibration could be developed by using high-performance computing and artificial intelligence through correlating device parameters, such as SS, mobility, threshold voltage, charge trap-relaxation time, band gap, and layer number information from measured on/off ratio. In addition, high-frequency ac impedance testing, electronic resonance-shifting, and noise spectral information could also be useful for scanning and extracting the device channel-oxide and contact interface quality in detail to provide additional input that can make the device calibration more fruitful. [5, 22, 31] Therefore, there are excellent opportunities for future work on the batch-processing and scaling of PFET sensors, code development, and its immense potential for real-time uses.

2.7 Influence of Al_2O_3 Layer Thickness on the Response Transient Pattern and Its Optimization

A stable, monotonic sensor response is needed to eliminate the ambiguity for real-time response% calculation. The stable ideal exponential output is generally observed when a single mechanism is involved during sensing without disturbance from other sources, such as leakage current from a gate oxide defect. In this section, a theoretical model is provided to study the influence of gate oxide (Al_2O_3) thickness on the patterns of response transients, and this model is supported by experimental data. To verify the role of Al_2O_3 for obtaining a stable response, PFETs with varied Al_2O_3 thicknesses

were fabricated and characterized while keeping the other device components the same. As shown in Figure 5a and b, the lead ion responses of the PFET without an Al_2O_3 layer or with a 3-nm Al_2O_3 layer showed bidirectional transients with spike-like features at the injection points. Neither spikes nor bidirectional responses are desirable for real-time monitoring of lead ions because they significantly hamper the calibration and confuse the micro-processor during signal analyses. When comparing the PFET with the 5-nm Al_2O_3 passivation layer (Figure 3d), both the spike-like features and bidirectional transients are almost absent. Of course, the calculated response% is much lower compared with sensors with thinner Al_2O_3 layers, but the signal is one-directional and very uniform. Figure 5c shows the effect of Al_2O_3 thickness on the PFET sensor responses for 1 ppb lead ion solution. The response% decreases when the thickness of the Al_2O_3 increases due to the increased distance between the sensing site and the FET channel. The bidirectional features for 0 and 3 nm Al_2O_3 sensors could be attributed to the competition between the charge transfer and the electrostatic gating effect, which cause signal changes in opposite directions. Figure 5d and e show the structures of PFETs without and with passivation, respectively. When lead ions are present in water, the PFET without passivation faces a combination of direct charge transfer (red arrow) and electrostatic gating (thunder sign), which are opposite to each other and thus outputs a bidirectional response. The PFET with 3 nm Al_2O_3 could still experience leakage current through the relatively thin Al_2O_3 layer due to the charge transfer, but a bidirectional response still occurs. Increasing the Al_2O_3 layer to 5 nm could prevent the leakage current almost completely, which removes the influence of change transfer. Lead ions only cause the electrostatic gating effect for the PFET, resulting in one-directional responses, as shown in Figure 3d. The bidirectional responses were also reported for BP and transition metal dichalcogenide-based sensors, which has been insufficiently explained. [4, 18-20] The observed response transients for various Al_2O_3 thicknesses could be modelled through the superposition of several effects, such as electrostatic gating, electronic charge transfer, and leakage current through ion diffusion. As expected, the time constant of each phenomenon should be different and the direction of the transient would complement each other. Assuming Langmuir adsorption kinetics, we propose the following equation to fit the response transient ($R(t)$) by adopting these three simultaneous effects:

$$\boldsymbol{R(t) = R_{eq} + Ae^{-t/\tau_1} - Be^{-t/\tau_2} + Ce^{-t/\tau_3}} \quad (9)$$

where R_{eq} is the response value near the equilibrium of the response transient, and t is the measurement time instant; A, B, and C are respective fitting constants for three different effects identified through three different time constants, τ_1, τ_2 and τ_3. The sign (positive or negative) of the equation represents the direction of change in the response pattern. The fitted response transients for Al_2O_3 layers with 0-5 nm thicknesses for 1 ppb lead ion concentration is found in Figure 5f–h. As evident from the analysis, τ_1 is much smaller than τ_2 and τ_3 for each case. This initial rapid increase in response (τ_1) could be ascribed to electrostatic gating after the initial adsorption of the positive lead ions at the cysteine interface and the rapid creation of opposite charge inside the BP channel. The second contribution from τ_2 is opposite to and slower than the previous effect (τ_1), because charge carriers have to pass through the Al_2O_3 gate oxide in the form of leakage current. The third contribution (τ_3) is much slower than the previous two and could be governed by the additional lead ion adsorption that is diffusion-controlled inside the solution. Upon systematic increase in Al_2O_3 thickness, the contribution of the second component diminishes due to the decrease in leakage current, resulting in the transition of the response transient from bidirectional to unidirectional. Therefore, passivation is essential not only for preventing from BP oxidation but also for obtaining a stable ideal response. The passivated PFETs with a cysteine probe showed a higher response and excellent selectivity than the results in the literature, as compared in Table S1 of Supporting Information. Using high-k dielectrics and larger gate oxide thickness, the current modulation could be accomplished more efficiently by modulating a small gate voltage with a reduced leakage current.[32,33] In future studies, better dielectric material, e.g., HfO_2, for the top gate passivation to replace Al_2O_3 could be explored to further improve the sensing performance of BP FET devices.

Conclusions

We have discussed and addressed several technical issues and challenges regarding the PFET sensor for real-life implementation. Using the MOSFET structure and band-bending model near the gate oxide channel interface, we developed a theoretical model for layer-dependent response. The model shows that atomically thin BP can provide higher response% due to excellent gate control by harvesting minority charge carriers in the channel. We have demonstrated improved mechanical exfoliation and the transfer of atomically thin BP nanosheet with selected-area exfoliation. The selected-area exfoliated PFETs had a narrow thickness distribution of thin BP layers, higher on/off ratio, and lower SS value, and showed better response for lead ions compared with random-area-based devices that had BP sheets with a broader distribution and higher average thickness.

The sensing measurements were carried out in the linear region to avoid a carrier switching near the threshold region and to achieve detection capability for a wide range of lead ion concentrations; we discussed a qualitative statement as to why the linear region is preferable for sensing in this respect. Using cysteine as the top gate (5 nm) probe, a large response% and excellent selectivity was achieved for ~1-400 ppb lead ion with a one-direction response transient, whereas, the samples from the random area showed a lower response due to a smaller on/off ratio and higher SS value at the linear region. The observed response% of the current BP devices towards lead ion detection was found to be much better than the results reported in the literature. This outstanding sensing performance was achieved due to the excellent electrostatic control over the atomically thin nature of the BP device, which was achieved by selected-area exfoliation and rapid processing by minimizing the top surface oxidation. A band gap dependence on the response model combined with band-bending modelling near the channel-gate oxide interface was introduced for the gated FET structure to explain the layer-dependent response.

For device variation issues and correlation with the evaluated response%, the measured on/off ratios were correlated with sensing parameters to build a calibration model for a certain range. We suggest that this calibration model could be more efficient by using high-performance AI computation that combines fabrication parameters, device simulation, and electronic parameters such as dc measurement (SS, mobility, threshold voltage), ac measurement (gate oxide quality, phase and resonance information), and noise information (defect information at the channel-gate oxide interface). We also have modelled the nature of the response transients (bidirectional/spike-like and exponential) upon variation of top gate oxide thickness. Using Langmuir adsorption isotherm, a superposition effect of electrostatic gating, charge transfer, and leakage current through metal ion diffusion was integrated to fit the response transients. The calculated time constant and direction of each phenomenon differed between each other. We observed that by increasing top gate thickness from 0 to 5 nm, the response transients' change from non-ideal spike/bidirectional nature to ideal exponential response feature is highly desired for real-time controllers to calculate the stable response% from the sensors.

Methods

Materials and Device Fabrication Details

Black phosphorus (purity 99.99%) bulk crystals (HQ Graphene, Groningen, Netherlands (Europe)) were mechanically exfoliated with our position-tracked, selected-area mechanical exfoliation, and thin BP nanosheets were transferred onto gold interdigitated electrodes pre-fabricated on highly doped silicon wafers (<100> oriented Si and 300 nm thermally grown SiO_2 as the back gate). The detailed process of exfoliation is schematically explained in Figure 1a. Au interdigitated electrodes (inter-finger spacing ~1.5 um) were designed and fabricated with photolithography using a Heidelberg Maskless Aligner MLA 150. After transferring the BP flakes, a subsequent annealing treatment (~200 ºC for 1 hr) combined with rapid transfer to an ALD chamber (Savannah 100, Cambridge Nanotech) was performed to construct the top gate oxide (Al_2O_3) for surface passivation. The thickness of the Al_2O_3 varied from 3 nm to 5 nm with a predefined optimized recipe by increasing the number of deposition cycles. The temperature for Al_2O_3 growth was maintained at 100 ºC. A gold sputter coater (RF K550X, Emitech gold nanoparticles) was used to deposit gold nanoparticles on the PFET samples. Saturated L-Cysteine solution (~5 µl) was dropped on the active surface of the PFET sensor, which was kept inside a closed air-tight desiccator for 1 hr. Finally, the device was thoroughly rinsed with ultrapure water and dried with compressed dry air flow to remove the excess chemicals. The sensing test was conducted in a 3D-printed test cell, with a diced PDMS micro-reservoir integrated on the sensor's active area.

Morphological, Surface, Spectroscopic, and Electronic Characterization*:*

A S-4800 UHR Hitachi Field Emission Scanning Electron Microscope (FESEM) was used for characterizing the surface morphology at an accelerating voltage 10 kV. The atomic force microscopy (AFM) characterization was conducted with a 5420 AFM, Agilent Technology (Cantilever PPP-NCH) in ACAFM mode. Raman spectroscopy was performed with a Renishaw Raman Spectrometer (1000B). A Keithley 4200 Semiconductor Characterization System (SCS) was used for electronic characterization of the FETs at ambient temperature.

Heavy Metal Ion Solution Preparation in Ultrapure Water

Various metal chloride or nitrate salts (from Sigma-Aldrich) were used to prepare the Pb^{2+}, Hg^{2+}, Cd^{2+}, Ag^{+}, Fe^{3+}, Na^{+}, and Mg^{2+} solutions. Since the primary forms of Arsenic within a 2–11 pH range can be $H_2AsO_4^-$, $HAsO_4^-$ in natural water, we used disodium hydrogen arsenate Na_2HAsO_4 from Sigma-Aldrich to prepare the test solution. Inductively coupled plasma mass spectrometry (ICPMS) was used to quantify the concentrations of prepared metal ion solutions, with an error less than 5%. To remove larger particles, algae, and other biological contaminants in the tap water, the water samples were filtered with Millipore filters before the sensing tests and then lead ion solutions of different concentrations were added to mimic the real situation. The tap water samples were further tested with ICPMS to confirm the concentration of lead ions.

Conflicts of interest

There are no conflicts to declare.

Acknowledgements

This work was supported by the U.S. National Science Foundation under grant number CBET-1606057. J. H. Chen acknowledges support by (while serving at) the U.S. National Science Foundation. The authors also acknowledge the technical support and instrumentation facilities at the Advanced Analysis Facility and Global Water Center of the University of Wisconsin-Milwaukee.

Notes and references

1 Y. Liu and K.-W. Ang, *ACS Nano*, 2017, **11(7)**, 7416.
2 D. Akinwande, N. Petrone and J. Hone, *Nat. Commun*., 2014, **5**, 5678.
3 S.M. Cui, H. Pu, S.A. Wells, Z.H. Wen, S. Mao, J. Chang, M.C. Hersam and J. Chen, *Nat. Commun*. 2015, **6**, 8632.
4 P. Li, D. Zhang, J. Liu, H. Chang, Y.E. Sun and N. Yin, *ACS Appl. Mater. Interfaces*, 2015, **7(44)**, 24396.
5 J. Chang, A. Maity, H. Pu, X. Sui, G. Zhou, R. Ren, G. Lu and J. Chen, *Nanotechnology*, 2018, **29(37)**, 375501.

6 L. Li, Y. Yu, G. J. Ye, Q. Ge, X. Ou, H. Wu, D. Feng, X. Chen and Y. Zhang, *Nat. Nanotechnol*., 2014, **9**, 372.
7 Y. Cai, G. Zhang, Y.W. Zhang, *Sci. Rep.,* 2014, **4**, 6677.
8 M. Pumera, *Mater. Today.*, 2011, **14(7)**, 308.
9 A. Maity, X. Sui, C. R. Tarman, H. Pu, J. Chang, G. Zhou, R. Ren, S. Mao and J. Chen, *ACS Sens*., 2017, **2(11)**, 1653.
10 X. Chen, H. Pu, Z. Fu, X. Sui, J. Chang, J. Chen and S. Mao, *Environ. Sci. Nano*, 2018, **5(8)**, 1990.
11 G. Lu, L. Ocola and J. Chen, *Nanotechnology*, 2009, **20(44)**, 445502.
12 J. Kang, W. Cao, X. Xie, D. Sarkar, W. Liu and K. Banerjee, Proc. SPIE 9083, *Micro- and Nanotechnology Sensors, Systems, and Applications* VI. 2014, 908305 SPIE.
13 M. Pumera, TrAC Trends in *Anal. Chem.*, 2017, **93**, 1.
14 V. Tayari, N. Hemsworth, I. Fakih, A. Favron, E. Gaufrès, G. Gervais, R. Martel and T. Szkopek, *Nat. Commun.*, 2015, **6**, 7702.
15 D. Hanlon, C. Backes, E. Doherty, C. Cucinotta, N. Berner, C. Boland, K. Lee, A. Harvey, P. Lynch, Z. Gholamvand, S. Zhang, K. Wang, G. Moynihan, A. Pokle, Q. Ramasse, N. McEvoy, W. Blau, J. Wang, G. Abellan, F. Hauke, A. Hirsch, S. Sanvito, D. O'Regan, V. Duesberg and J. Coleman, *Nat. Commun*., 2015, **6**, 8563.
16 W. Lu, H. Nan, J. Hong, Y. Chen, C. Zhu, Z. Liang, X. Ma, Z. Ni, C. Jin and Z. Zhang, *Nano Res*., 2014, **7(6)**, 853.
17 Z. Yang, J. Hao, S. Yuan, S. Lin, H. Yau, J. Dai, S. Lau. *Adv. Mat.*, 2015, **27(25)**, 3748.
18 P. Li, D. Zhang, C. Jiang, X. Zong and Y. Cao, *Biosens. Bioelectron.*, 2017, **98**, 68.
19 O. Kwon, H. Song, S. Park, S. Lee, J. An, J. Park, H. Yang, H. Yoon, J. Bae, T. Park and J. Jang, *Nano Lett*., 2015, **15(10)**, 6559.
20 G. Zhou, J. Chang, H. Pu, K. Shi, S. Mao, X. Sui, R. Ren, S. Cui and J. Chen, *ACS Sens*., 2016, **1(3)**, 295.
21 J. Wood, S. Wells, D. Jariwala, K. Chen, E. Cho, V. Sangwan, X. Liu, L. Lauhon, T. Marks and M. Hersam, *Nano Lett*., 2014, **14(12)**, 6964.
22 A. Maity, X. Sui, B. Jin, H. Pu, K. Bottum, X. Huang, J. Chang, G. Zhou, G. Lu and J. Chen, *Anal. Chem*., 2018, **90(24)**, 14230.
23 R. Seenivasan, W.Chang**,** S. Gunasekaran, *ACS Appl. Mater. Interfaces*, 2015, 7, 29, 15935.
24 V. Tran, R. Soklaski, Y. Liang and L. Yang, *Phys. Rev. B*, 2014, **89**, 235319.
25 B. Streetman and S. Banerjee, Solid State Electronic Devices. 7th ed. 2014: Pearson.
26 S.M. Sze, Physics of Semiconductor Devices. 1969: Wiley-Blackwell.
27 D. Sarkar, W. Liu, X. Xie, A.C. Anselmo, S. Mitragotri and K. Banerjee, *ACS Nano*, 2014, **8(4)**, 3992.
28 M. Acik and Y.J Chabal, *J. Mater. Sci. Res*, 2013, **2**, 101.
29 Diabetes.co.uk. Importance of Coding. (accessed April 4, 2019); Available from: https://www.diabetes.co.uk/diabetes_care/the-importance-of-coding.html.
30 DiabetesMonitor.com. (accessed April 4, 2019); Available from: http://www.diabetesmonitor.com/glucose-meters/coding-is-important-for-glucose-monitors.htm.
31 G. Zheng, X. Gao and C. Lieber, *Nano Lett.*, 2010, **10(8)**, 3179. S. Das, W. Zhang, M. Demarteau, A. Hoffman and A. Roelofs, *Nano Lett*., 2014, **14**, 5733.
32 X. Li, Z. Yu, X. Xiong, T. Li, T. Gao, R. Wang, R. Huang and Y. Wu1, *Sci. Adv*., 2019, **5**, eaau3194.
33 X. Li, X. Xiong, T. Li, T. Gao and Y. Wu, *IEEE Electron Device Lett*., 2018, **39 (12)**, 1955.
34 S. Mao, J. Chang, H. Pu, G. Lu, Q. He, H. Zhang, J. Chen, *Chem. Soc. Rev*., 2017, **46**, 6872.
35 X. Ge, Z. Xia, S. Guo, *Adv. Funct. Mater*.2019, **29**, 1900318.
36 J. Zhou, Z. Li, M. Ying, M. Liu, X. Wang, X. Wang, L. Cao, H. Zhang and G. Xu, *Nanoscale*, 2018, **10**, 5060-5064.
37 L. Zhou, C. Liu, Z. Sun, H. Mao, L. Zhang, X. Yu, J. Zhao, X. Chen, *Biosens. Bioelectron.*, **15**, 2019, 140.
38 Y. Chen, R. Ren, H. Pu, J. Chang, S. Mao, J. Chen *Biosens. Bioelectron.,* **89**, 2017, 505.
39 Y. Zhao, Ye-Hua Z. Zhen, Z. Yi-Hong, T. Wei Tao, Y. Chen, 2018, *Anal. Chem*., **90**, 2018, 3149.
40 C. C. Mayorga-Martinez, Z. Sofer, M. Pumera, *Adv. Mater*. **54,** 2015, 14317.
41 C. Cobbett, P. Goldsbrough, *Annu. Rev. Plant Biol.* **53,** 2002, 159.
42 K. Fischer, *Water Air Soil Poll.* **137**, 2002, 137, 267.
43 T. M. Vadas, B. A. Ahner, *J. Environ. Qual.* 2009, **38**, 2245.
44 S. Wang, C. N. Mulligan, *Environ. Geochem. Health*, 2013, **35**, 111.
45 F. Jalilehvand, N. S. Sisombath, A. C. Schell, G. A. Facey, Inorg. Chem., 2015, **545**, 2160.
46 B. J. Fuhr, D. L. Rabenstein, *J. Am. Chem. Soc.* 1973, **95**, 6944.
47 K. Chen, G. Lu, J. Chang, S. Mao, K. Yu, S. Mao, S. Cui, J. Chen, *Anal. Chem*., 2012, **849**, 4057.
48 M. Chhowalla, D. Jena, H. Zhang, *Nature Reviews Materials,* 2016*,* **1**, 1.